Spring 5-6-2022

Computational analysis of a Mn-based electrocatalyst with primary amine substituents in the secondary coordination sphere for CO2 reduction

Erin Urban
Binghamton University--SUNY, eurban1@binghamton.edu

COMPUTATIONAL ANALYSIS OF A MN-BASED ELECTROCATALYST WITH PRIMARY AMINE SUBSTITUENTS IN THE SECONDARY COORDINATION SPHERE FOR CO_2 REDUCTION

BY

ERIN URBAN

HONORS THESIS

Submitted in partial fulfillment of the requirements for
The degree of Bachelor of Science in Chemistry
In Harpur College of
Binghamton University
State University of New York
2022

Submitted in partial fulfillment of the requirements for
The degree of Bachelor of Science in Chemistry
In Harpur College of
Binghamton University
State University of New York
2022

May 6, 2022

Julien Panetier, Faculty Advisor
Department of Chemistry, Binghamton University

John Swierk, Member
Department of Chemistry, Binghamton University

Alistair Lees, Member
Department of Chemistry, Binghamton University

Abstract

The purpose of this research was to report the mechanism for the two-electron, two-proton conversion of CO_2 to CO and H_2O using a manganese(I) electrocatalyst, $Mn(L)(CO)_3Br$ (where L = bipyridyl ligand with aryl-amine moieties installed at the 6 position of 2,2'-bipyridine), synthesized by the Jurss group, including any other competing reactions, such as the hydrogen evolution reaction (HER). The "protonation-first" and "reduction-first" pathways were considered for CO_2RR. Density functional theory (DFT) calculations were performed to determine the redox potentials and Gibb's free energies for each step in the mechanism for CO_2RR and HER. Herein, we show that the "reduction-first" pathway is the most favorable in the production of CO, especially under high applied potential (i.e., high overpotential regime used experimentally). Additionally, this work confirms the selectivity of $Mn(L)(CO)_3Br$ for CO production over H_2 formation. Repeating these calculations with a larger basis set and focusing future research on additional functionalized ligands will be an improvement upon this work.

Acknowledgments

I want to express gratitude to my advisor, Dr. Panetier, everyone in the Panetier group, the Binghamton University Chemistry Department, my family, and my friends for all their support in completing this research project.

Table of Contents

1. Introduction

Current environmental issues, such as global climate change, related to the increase in anthropogenic greenhouse gas emissions have emerged over the past few decades. To reduce the amount of greenhouse gasses that have been released into the atmosphere, new technologies have begun to be studied.[1] Some of these studies focus on converting greenhouse gasses into less environmentally harmful compounds, or, for a more useful purpose, liquid fuels. One of the greenhouse gasses, carbon dioxide, has a considerable kinetic energy barrier that makes it difficult to convert into value-added chemicals.[1] Therefore, efficient chemical catalyst technologies are an important field of study to reduce the environmental impacts of excess carbon dioxide. These catalysts allow the CO_2 reduction reaction (CO_2RR, **Figure 1**) to occur at a faster rate and create products such as carbon monoxide or formic acid by suppressing the competing hydrogen evolution reaction (HER).[1]

$$CO_2 + 2H^+ + 2e^- \rightleftharpoons CO + H_2O$$

Figure 1. Chemical reaction equation for CO_2 to CO and H_2O through a two-proton, two-electron reaction.

Previous research into catalysts for this reaction has found that transition metals, such as rhenium and manganese, with bipyridine (bpy) ligands may be effective because of their tunable properties and well-defined active sites.[1,2] Additionally, changing the functional groups in the secondary coordination sphere of these catalysts may increase their effectiveness and allow the faster conversion of CO_2 to valuable chemicals.[1,2] Overall,

creating efficient catalysts that can reduce the energy of the CO_2RR can improve both the environment and the economy by reducing greenhouse gas emissions and creating a circular fuel economy by converting CO to methanol, DME, or Fischer-Tropsch fuels.[3]

Research into CO_2 reduction catalysts with rhenium transition metal began in the 1980s as the issue of greenhouse gas accumulation was first recognized.[1] This research sought to create a homogenous catalyst efficient enough to decrease the energy required for the CO_2 reduction reaction (CO_2RR). The Lehn catalyst, $Re(bpy)(CO)_3Cl$ (bpy = 2,2'-bipyridine), published in a 1984 research paper, was the first in a series of rhenium catalysts that was able to reduce CO_2 to CO.[4] This catalyst was first produced in a photochemical system in which light irradiation was used to drive the reaction. The researchers then sought to use an electrochemical approach to improve the activity. They thought that by successfully creating a catalyst that could reduce the potential of CO_2RR, chemical conversion and energy storage could be improved.

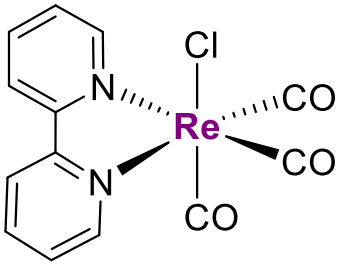

Lehn catalyst

Figure 2. Structure of Lehn catalyst, first synthesized in the 1980s.[4] Rhenium-based electrocatalyst for CO_2-to-CO conversion, which set the basis for rhenium catalysts in this field.

Lehn and co-workers also showed that formate production was suppressed due to the co-coordinating anions present in the complex and that the CO_2 reduction process occurred in another site on the complex. Therefore, this catalyst was found to be highly selective for CO production. While the reaction was known to include a reduction of CO_2 to CO and a regeneration of the catalytic complex, the intermediates and chemical steps for CO_2RR were not known in the 1980s. Further research was performed following this work to probe the reaction mechanism. Additionally, Lehn *et al.* suggested the possibility of ligand modification to improve the efficiency of Re(bpy)$(CO)_3$Cl. While much was unknown about this catalytic compound, it set the basis for future research into rhenium-based catalysts for CO_2RR.[4]

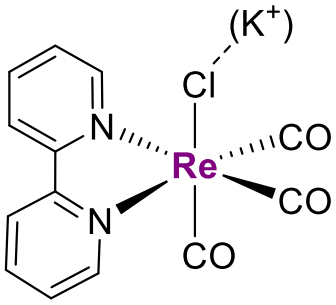

Keith *et. al*

Figure 3. Structure of the Keith *et al.* catalyst, published in 2013.[5] Rhenium-based electrocatalyst for CO_2RR to CO with K^+ counterion interacting with the complex.

Continuing the study of rhenium-based CO_2 reduction catalysts, computational chemistry tools were utilized to propose a reaction mechanism for CO_2RR. Finding the mechanistic path of catalysis provides great information for improving catalysts or creating better ones. A study done by Keith *et al.* in 2013 used both experimental and principles of quantum chemistry to study the pathway of the *fac*-Re(bpy)$(CO)_3$Cl complex to improve

upon the work done by the Lehn group and fill in the gaps of knowledge about the mechanistic pathway.[5] The importance of the research done by Keith *et al.,*[5] like the significance of this research project, comes from reducing the amount of CO_2 in the atmosphere and creating more sustainable fuel sources and commodity chemicals. Specifically, focusing on the production of CO in this reduction reaction could lead to the creation of methanol and Fischer-Tropsch fuels.

To find the mechanistic pathway for the *fac*-Re(bpy)$(CO)_3$Cl catalyst, several calculations were done to determine the one-electron reduction potentials, nonaqueous pKa's, free energies values for reactions, and reaction barrier values. These researchers predicted a two-electron, two-proton dependent reduction process, which would be the most efficient pathway. Keith *et al.* performed density functional theory (DFT) calculations using the B3LYP exchange-correlation function to support their hypothesis. To optimize the geometries during calculations, the 6-31+G** basis set was utilized for all atoms except K and Re, which instead used the LANL2DZ effective core potentials (ECPs) and their corresponding basis sets. Experimentally, these researchers determined the reduction potential using a saturated calomel electrode (SCE) in acetonitrile to compare with the computationally derived data.[5]

Due to this research, several important steps in the mechanism were discovered, such as interactions with the solvent and the stability of the intermediates. The components needed for reaction, such as protons, electrons, and Brønsted acids, were developed by studying how each of these species interacted with the complex to allow CO_2RR to occur. An entire mechanism for CO_2RR using this catalyst was proposed in this study at different potentials, which was used to explain the selectivity of CO production. Another major

result of this study included the electronic structure of this catalyst, which was produced from both experimental and computational methods, improving the knowledge about this catalyst and adding more to this study than if only one method was employed. Finally, this paper mentioned the start of using earth-abundant Mn instead of rarer and more expensive Re. Finding the mechanistic pathway for Mn could improve the cost-effectiveness of this research and the CO_2 reduction process. Overall, the researchers hoped for a future focus on catalysts that will continue to reduce the reaction barriers at lower reduction potentials by researching various proton donors and the electrostatic effects that substituted ligands have on the catalyst.[5]

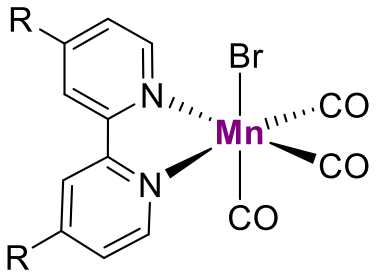

Bourrez catalyst
R = H (1) or Me (2)

Figure 4. Structure of the Bourrez catalyst, published in 2011.[6] Manganese-based electrocatalyst for CO_2RR to CO under mild conditions. Two different catalysts were studied with hydrogen or methyl attachments to the bipyridine ligand.

One of the first Mn-based catalysts, $Mn(bpy)(CO)_3Br$ (bpy = 2,2'-bipyridine), for electrochemical CO_2 reduction to CO was reported by the Bourrez group in 2011 (**Figure 4**).[6] This was done after considerable research into previous CO_2 reduction catalysts made from Re, Ru, and Os. Mn was chosen as the metal center for this catalyst due to its similar properties to Re (group 7 transition metal). Mn is also the third most abundant transition

metal in the Earth's crust at 0.1%.[6] To study this Mn-based catalyst, cyclic voltammetry was utilized and showed that $Mn(bpy)(CO)_3Br$ goes through two successive irreversible reductions. Upon addition of CO_2 into the reaction vessel, no change was observed until H_2O was also added. This was due to the stabilization of the complex from hydrogen bonding interaction and the presence of a proton source which allowed the C-O bond cleavage step. It was found that the number of electrons consumed during the reduction reaction directly correlated with the amount of CO produced. The mechanism for this reaction was proposed using cyclic voltammetry, IR spectroscopy, and UV-Vis data. In this mechanism, the formation of dimers of the catalyst can be seen upon bromide dissociation. Overall, compared to the Lehn catalyst, $Mn(bpy)(CO)_3Br$ switched the potential by 400 mV, reducing the overpotential and having very similar selectivity and Faradaic efficiency for CO production. The authors conclude this paper by suggesting an investigation into the addition of ligands to improve the overall performance of Mn catalysts.[6]

Following the creation of the efficient Mn parent electro- and photocatalyst, $Mn(bpy)(CO)_3Br$ (**Figure 4**), numerous research groups continued to study how manganese-based complexes could be improved by including functional groups in the secondary coordination sphere. Specifically, the Jurss group at the University of Mississippi developed a series of manganese(I) complexes that include aniline groups at the *ortho*- (**1-Mn**), *meta*- (**2-Mn**), or *para*- (**3-Mn**) position of the amino-phenyl ring substituent (**Figure 5**).[2]

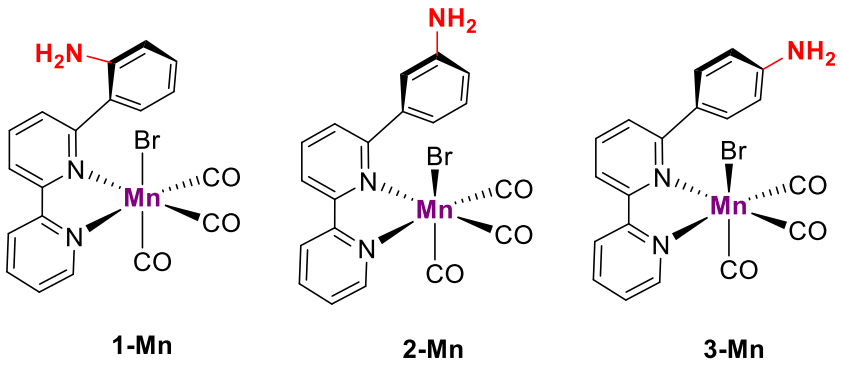

Figure 5. Catalysts synthesized by the Jurss group. A primary amine is located at the *ortho*- position for **1-Mn**, the *meta*- position for **2-Mn**, and the *para*- position for **3-Mn**. Catalyst **1-Mn** will be the focus of this research project.[2]

Finding which of these catalytic isomers was the most efficient and finding the possible reasoning for this efficiency was the objective of this study. Functional groups in the secondary coordination sphere were formerly hypothesized to control the product selectivity. Previously, research has shown that a proton source is required for this catalyst to convert CO_2 to CO/formic acid, and the reduction may occur through either the "protonation-first" or "reduction-first" pathways.[2]

This study by the Jurss group used experimental methods, such as cyclic voltammetry, to find the efficiency of the series of catalytic compounds. Trifluoroethanol (TFE), a weak Brønsted acid, was used as a proton source to drive catalysis. From cyclic voltammetry, the catalytic peaks were identified to be around -1.6 V and -2.2 V for the "protonation-first" and "reduction-first" pathways, respectively. It was found that the positioning of this group affected the catalyst's efficiency by the ability of hydrogen bonding interactions, and these interactions were able to lower the energy needed for the "protonation-first" pathway (**Figure 6**). These catalysts were selective towards CO

production at higher concentrations and HCO_2H at lower concentrations, which is highly useful due to the possibility of choosing the product being created. Overall, this series of Mn complexes are significantly more active catalysts than the original Re catalysts, in terms of overpotentials and turnover frequency, and behave entirely differently.[1,2] While a reaction mechanism was proposed by the authors based on the previous knowledge of the parent catalyst, the turnover determining transition states and critical intermediates formed during catalysis for these new catalysts are unknown, which is the focus of this computational research project.

Research by the Jurss group shows that these manganese-based catalysts that feature functional groups in the secondary coordination spheres could lower the overpotentials and enhance the catalytic activity for CO_2-to-CO conversion. Experimental data indicates that the *ortho*-substituted -NH_2 catalyst, **1-Mn**, had the best catalytic results, including the lowest overpotential, high Faradaic efficiency ($\geq 70\%$), and highest turnover frequency.[2] The primary amine substituent improves catalytic activity by allowing hydrogen-bonding interactions during catalysis, which creates an overall stabilizing effect. Initial results showed that **1-Mn** has the closest amine group to the metal center, making the second-sphere catalytic enhancement for the lower energy "protonation-first pathway." Additionally, the amine substituent will interact with the bromide ligand in the *ortho*-substituted position, which expedites the formation of the catalytic species, making **1-Mn**

more advantageous than **2-Mn**, **3-Mn**, and the parent complex.[2,6]

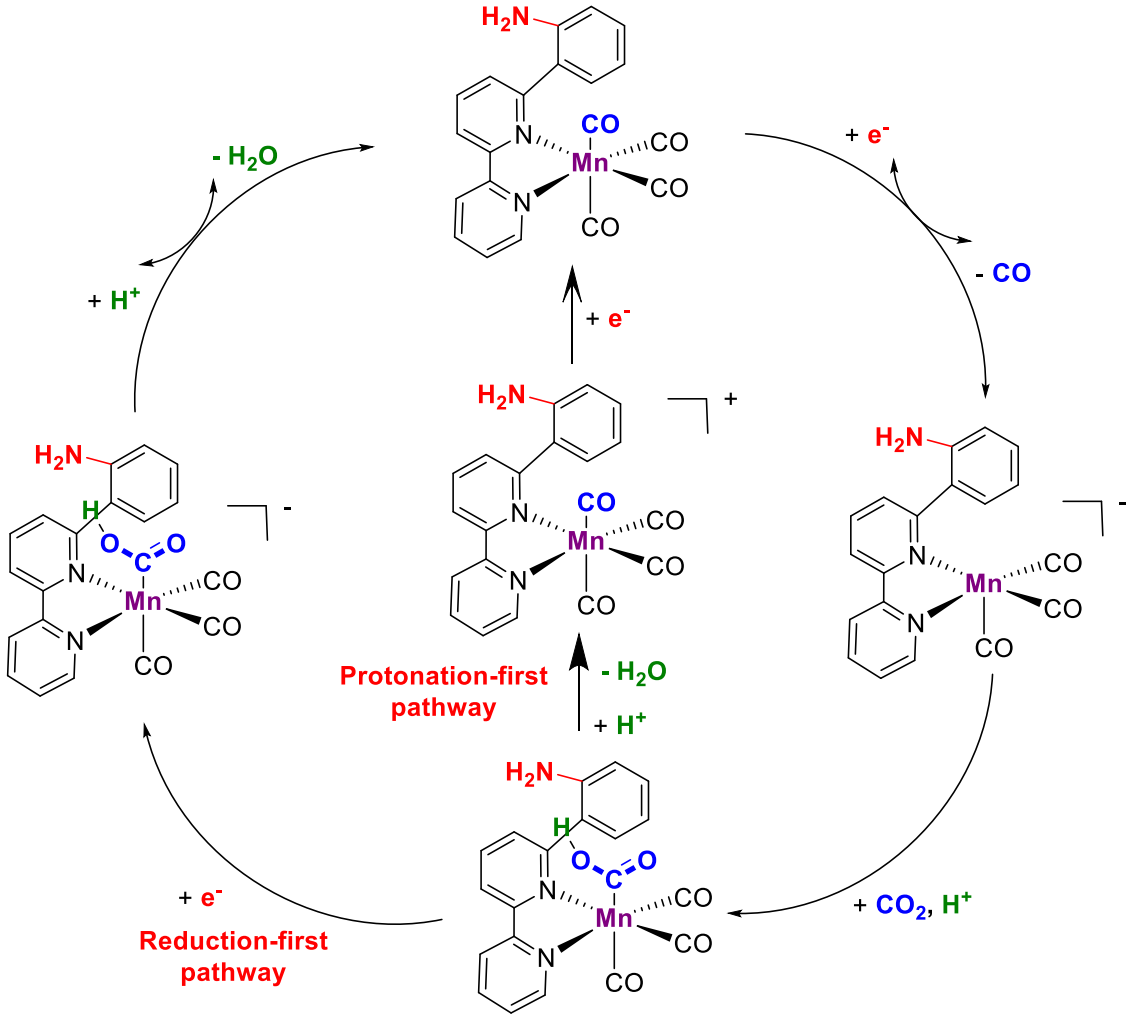

Figure 6. Catalytic cycle of **1-Mn** for CO_2 reduction through the two possible mechanisms: "protonation-first" versus "reduction-first" pathways.

This project aims to identify the energetic pathways of the $Mn(L)(CO)_3Br$ catalyst, where L is a functionalized-bipyridine ligand with the primary amine at the *ortho*-position **1-Mn**, for CO_2RR using computational methods. Previous experimental research has shown that this molecular species functions as the pre-catalyst, and after accepting two electrons and bromide dissociation, the five-coordinate species can bind and activate CO_2. After forming the metallocarboxylic acid intermediate, the reaction can proceed through two

mechanisms, the "protonation-first pathway" or the "reduction-first pathway," depending on the reaction conditions (**Figure 6**).

Studying and comparing the mechanisms of these two pathways and the associated amounts of energies for these two reactions can give insight into the most favorable process for CO_2 reduction using this catalyst. Therefore, one main objective of this research project is to find which pathway is the most favorable for CO production and compare it to the competing hydrogen evolution reaction (HER).

2. Computational Details

Electronic structure calculations were performed to probe the reaction mechanism for CO_2-to-CO conversion and H_2 formation using **1-Mn**. DFT calculations were performed using Gaussian 16 software along with the ωB97X-D functional and the SMD solvation model (i.e., acetonitrile, $\varepsilon = 35.688$). Specifically, ωB97X-D is a range-separated hybrid functional, which includes empirical dispersion corrections. This type of functional is beneficial for studying both the kinetics and thermodynamics of reaction mechanisms for many different types of molecules, as it incorporates calculations for van der Waals forces, which are not always included in DFT functionals.[7] The basis set used for optimization was Def2-TZVP for Mn and Def2-SVP for all other atoms. These basis sets include calculations for split valence polarization, which uses the theory that during molecular bonding, it is the valence electrons that take part in the bonding. These valence electrons can be represented by one or more basis sets corresponding to each valence

atomic orbital, called valence double, triple, and quadruple.[8] For this project, split-valence and valence triple-zeta polarization are used.

Frequency and geometry optimization calculations were performed to calculate the two-electron, two-proton reduction pathway for CO_2RR and HER using **1-Mn**. Additionally, DFT calculations were completed to find the transition state, which featured a negative eigenvalue, and IRC calculations were performed to confirm these transition states. The energies were corrected by including zero-point and Gibbs free energy correction values. Using these values, calculations were done to determine Gibb's binding and dissociation energies (in kcal/mol), and the reduction potentials (in V) were calculated using Ferrocene/Ferrocenium as a reference. The ChemDraw software was utilized to visually represent the proposed pathways, including Gibbs free energy values and reduction potentials. The computational data for CO_2RR using **1-Mn** were compiled and compared with the competing HER.

3. Computational Results

3.1. First and Second Reduction Events

Calculated Gibb's free energies and reduction potentials quantitatively can provide an explanation of which steps and chemical species correspond to the turnover determining transition state (TDTS) and turnover determining intermediate (TDI).[9] Primarily, the first step in our proposed reaction mechanism corresponds to the formation of the one-electron reduced species (**Figure 7**). The calculated redox potential for this step is -1.83 V versus Fc^0/Fc^+. Following this initial reduction, bromide dissociates from the complex and is

thermodynamically accessible (ΔG = 1.7 kcal/mol). We hypothesize that bromide dissociation occurs after the first reduction, despite not being spontaneous. Then, the second reduction occurs to reduce the complex further and this redox potential was calculated to be -1.63 V. After this step in the mechanism, the catalytic complex was in its active catalyst form and was ready to perform the CO_2RR. Compared to the experimental reduction potentials, the first reduction potential was lower than the experimental data, -1.83 V (*cf.* -1.56 V). However, experimentally, the second reduction potential (*cf.* -1.64 V) agrees with the calculated value (*cf.* -1.63 V).

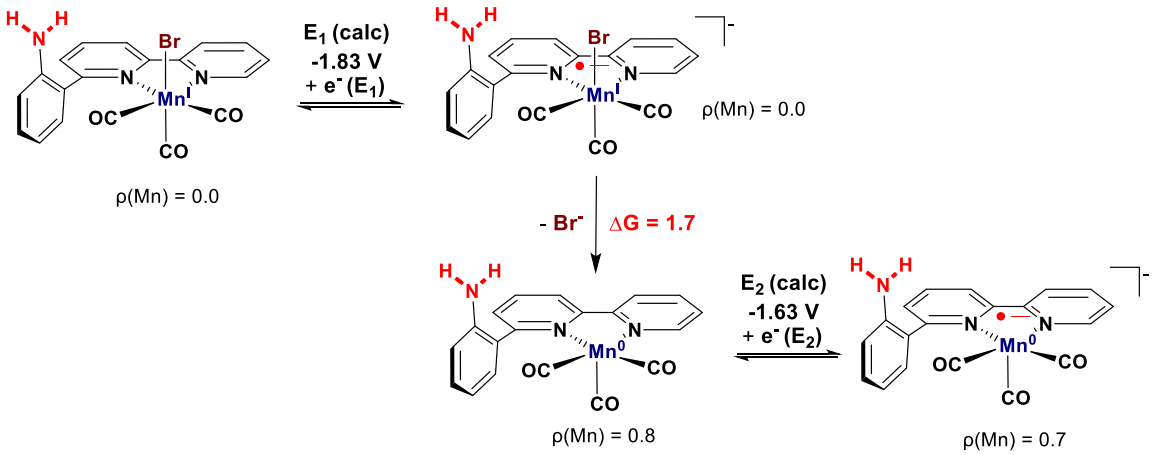

Figure 7. The computed Gibbs free energy values (in kcal/mol) for bromide dissociation and redox potential values (in V) for the first and second reductions, reported versus Fc^0/Fc^+, for **1-Mn**. Gibbs free energies were calculated using the ωB97X-D(SMD) level of theory. Additionally, the Mulliken spin values for each complex were included.

Electronic structure calculations were also employed to probe the ground state of the non-reduced, one- and two-electron reduced complexes. The Mulliken spin on the metal center is zero starting with the first species, consistent with manganese(I), d^6. Upon

reduction, the Mulliken spin remains zero, indicating that the first electron goes onto the π* orbital of the bipyridine ligand. However, bromine dissociates after this initial reduction, and the Mulliken spin on the metal increases to 0.8. This is consistent with a ligand to metal charge transfer during this dissociation to give a manganese(0) intermediate, d^7. The second reduction occurs and the Mulliken spin on the metal stays close to one, indicating that the second reduction is ligand-based. Overall, our calculations suggest that after the two sequential reductions, an electron is added onto the e_g orbital of the metal, and another is added to the π* orbital of the bipyridine ligand to form a manganese(0) ligand radical complex. After these steps in the mechanism, the catalytically active species is formed, and CO_2 can bind to the metal center.

3.2 Metallocarboxylic Acid Formation

Following the second reduction of the complex, CO_2 was added to the reaction mixture and bonded to the **1(red2)** species (**Figure 8**). The Gibbs free energy for CO_2 addition was calculated to be 3.9 kcal/mol. Overall, the CO_2 binding process was slightly uphill. The transition state energy, **1(TS1)**, was 11.7 kcal/mol, and the forward reaction energy of CO_2 binding was 7.1 kcal/mol with respect to the separated reactants. This could be due to the metal center activating CO_2 to allow the inert molecule to be involved in the reaction.

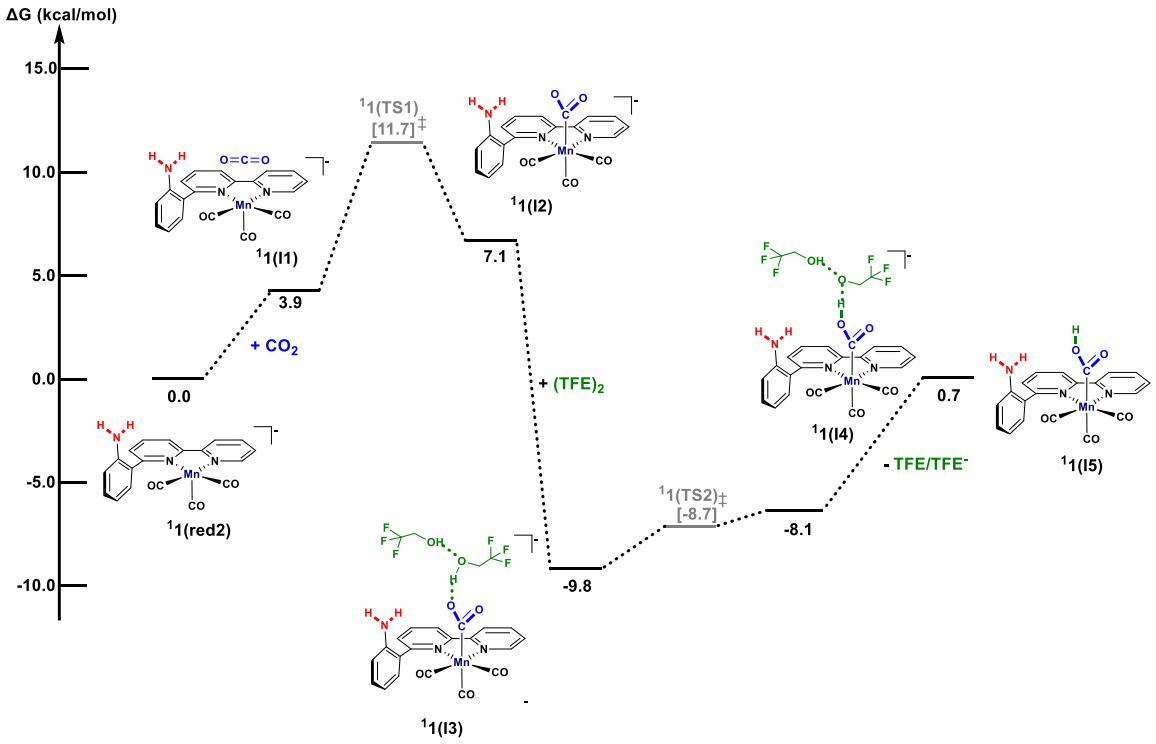

Figure 8. The computed Gibbs free energy values (in kcal/mol) and redox potential values (in V) reported against Fc^0/Fc^+ for metallocarboxylic acid formation. The catalyst goes through two main processes in this figure, carbon dioxide binding and sequential protonation. Gibbs free energies were calculated using the ωB97X-D(SMD) level of theory.

The next step in the mechanism included the addition of the protonation source. In this study, two trifluoroethanol (TFE) molecules were added to the reaction mixture to stabilize the electron density during the protonation steps. One of these molecules serves as the protonation source, while the other is used for stability purposes. Anhydrous CH_3CN was initially added as a proton source in the experimental work. However, the species went through no current increase until a weak Brønsted acid, TFE, was added to the reaction mixture, which is why this proton source was chosen for this computational work. The energy of the addition of the proton source was found to be -9.8 kcal/mol, and the transition

state, **1(TS2)**, to yield the metallocarboxylic acid intermediate, **1(I4)**, was -8.7 kcal/mol. The forward reaction for this protonation step was -8.1 kcal/mol. This process was much lower in energy than CO_2 binding due to the increased hydrogen bonding stabilization that TFE brings to the catalyst. One of the oxygens of the CO_2 was protonated by TFE to create H-O-C-O connected to the metal center of the catalyst. Finally, the conjugate base of the proton source is removed to leave the metallocarboxylic acid species (**1(I5)**, $\Delta G = 0.7$). The overall reaction for forming the metallocarboxylic acid species is slightly uphill.

3.3 "Protonation-First" Pathway versus "Reduction-First" Pathway

Sequentially, the mechanism can go through either two distinct pathways, the "protonation-first" or "reduction-first" pathways. The metallocarboxylic acid species, **1(I5)**, is the starting source for these next steps in the reaction. For the "protonation-first" path, the proton source, 2 TFE molecules, is added to the reaction mixture. Once again, the addition of the protonation source results in a lowering of the energy of the reaction. This was calculated to be -3.8 kcal/mol (**Figure 9**). The protonation results in forming a water molecule from the bond cleavage of C-O. This leaves carbon monoxide bound to the metal center of the catalyst. These two steps in the mechanism were calculated to have an increased amount of energy. The transition state, **1(TS4)**, was calculated to be 12.0 kcal/mol, and the forward reaction of water leaving was estimated to be 7.3 kcal/mol. Once again, the conjugate base of the proton is removed from the reaction mixture to leave a positively charged tetracarbonyl compound, **1(I7-P)**. The Gibbs dissociation energy of the conjugate base and water was calculated to be 11.3 kcal/mol, due to the decreased stability. Finally, this species goes through a reduction to return to a neutral charge. The redox

potential for this step was -1.5 V versus Fc^0/Fc^+, consistent with the catalytic peak identified experimentally at -1.6 V for the "protonation-first" pathway. Overall, the energy needed for this reaction mechanism was high, especially the formation of CO and water dissociation. This step had a reaction barrier of around 16 kcal/mol, which is higher in energy. Each of the steps in this pathway with the Gibb's free energy and redox potential values can be seen below in **Figure 9**. These calculations were performed at the experimental "high" regime, which was -1.95 V versus Fc^0/Fc^+.

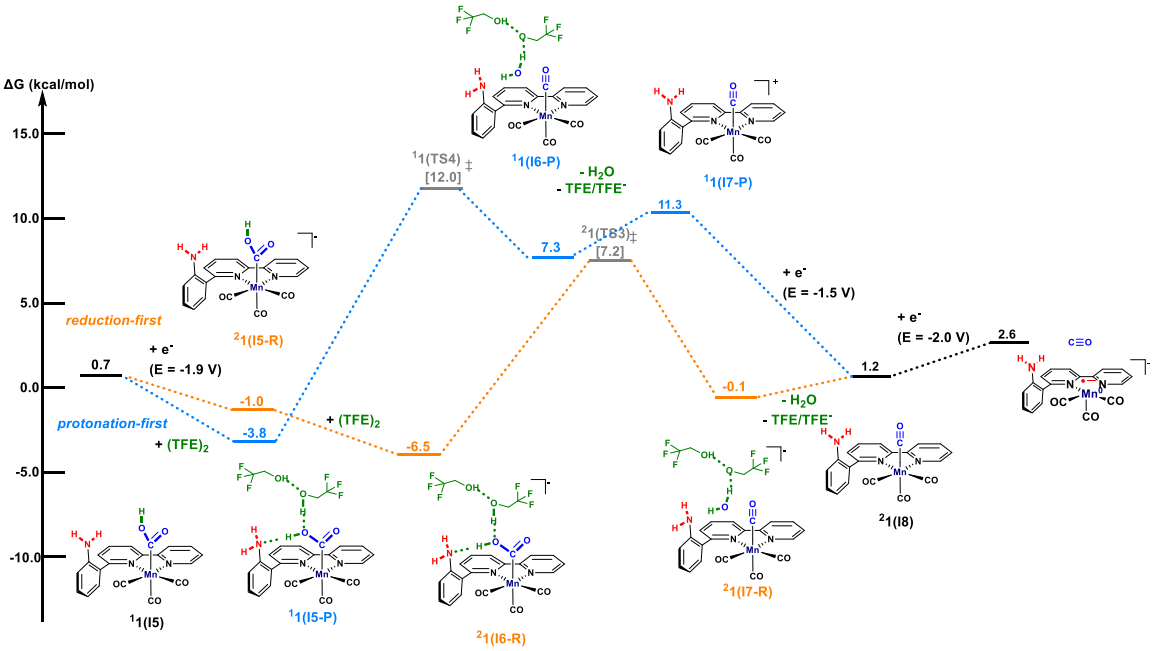

Figure 9. The computed Gibbs free energy values (in kcal/mol) and redox potential values (in V), reported against Fc^0/Fc^+, for the "protonation-first" and "reduction-first" pathways and the final reduction at an overpotential of -1.95 V. This is considered the high overpotential regime. Gibbs free energy values were calculated using the ωB97X-D(SMD) level of theory.

Alternatively, the "reduction-first" pathway starts by performing a reduction on the metallocarboxyllic acid species, **1(I5)**. The redox potential for this process was calculated to be -1.9 V, consistent with the catalytic peak observed experimentally at -2.2 V for the "reduction-first" pathway. The energy of the reduced metallocarboxyllic acid species, **1(I5-R)**, was calculated to be -1.0 kcal/mol. After this reduction, the proton source was added to the reaction mixture to perform the C-O bond cleavage and release water. Once again, this was a downhill process at -6.5 kcal/mol, **1(I6-R)**. The transition state energy for this step, **1(TS3)**, was calculated to be 7.2 kcal/mol, creating a reaction barrier of about 14 kcal/mol. The C-O bond cleavage was downhill, as the energy for the forward reaction was -0.1 kcal/mol, **1(I7-R)**. The last step for this reaction is the removal of the conjugate base, which was calculated to be 1.2 kcal/mol, a slightly uphill step. This left the bound carbonyl group on the catalytic species, **1(I8)**. Overall, this reaction was lower in energy than the alternative "protonation-first" pathway when performed at the high overpotential regime, -1.95 V versus Fc^0/Fc^+.

The final step of our proposed mechanism is the return to the active catalytic species, **1(red2)**, through another reduction. The redox potential for this reduction was calculated to be -2.0 V versus Fc^0/Fc^+, which creates uphill energy for the last step using the overpotential of -1.95 V versus Fc^0/Fc^+. The energy for the active catalyst species was calculated to be 2.6 kcal/mol, showing that this step of the reaction may be difficult to perform. This agrees with the experimental work, which found that a large overpotential was needed to complete the "reduction-first" pathway. Using a larger basis set in a future work may help lower some of the calculated Gibbs free energies and better explain the mechanism for the "reduction-first" and "protonation-first" pathways.

3.4 Overpotential Consideration

Experimentally, this reaction can be done at several different overpotentials, which can change the amounts of energy needed for the reaction steps for the "reduction-first" pathway. Besides the previously mentioned high regime of -1.95 V versus Fc^0/Fc^+, a low regime could also be used. The voltage of the low regime is -1.47 V versus Fc^0/Fc^+. For this low regime, it raises the energy for the "reduction-first" pathway's first step, **1(I5-R)**, to 10.6 kcal/mol (**Figure 10**). After this step, the addition of the proton source decreases the reaction energy to 5.1 kcal/mol for species **1(I6-R)**. Following, the energy for the transition state increases to 18.8 kcal/mol, and the energy forward reaction, species **1(I7-R)**, was calculated to be 11.5 kcal/mol. Finally, it also raises the energy of the carbonyl species' formation after removing the conjugate base species, **1(I8)**, to 10.6 kcal/mol. The overall reaction mechanism for the low regime with the calculated Gibbs free energies and redox values can be seen below in **Figure 10**. Under the low regime, the "protonation-first" pathway is more likely to happen, while the "reduction-first" pathway is more likely to occur under the high regime. These mechanisms agree with the experimental work about which pathway can proceed at the two different overpotential regimes.

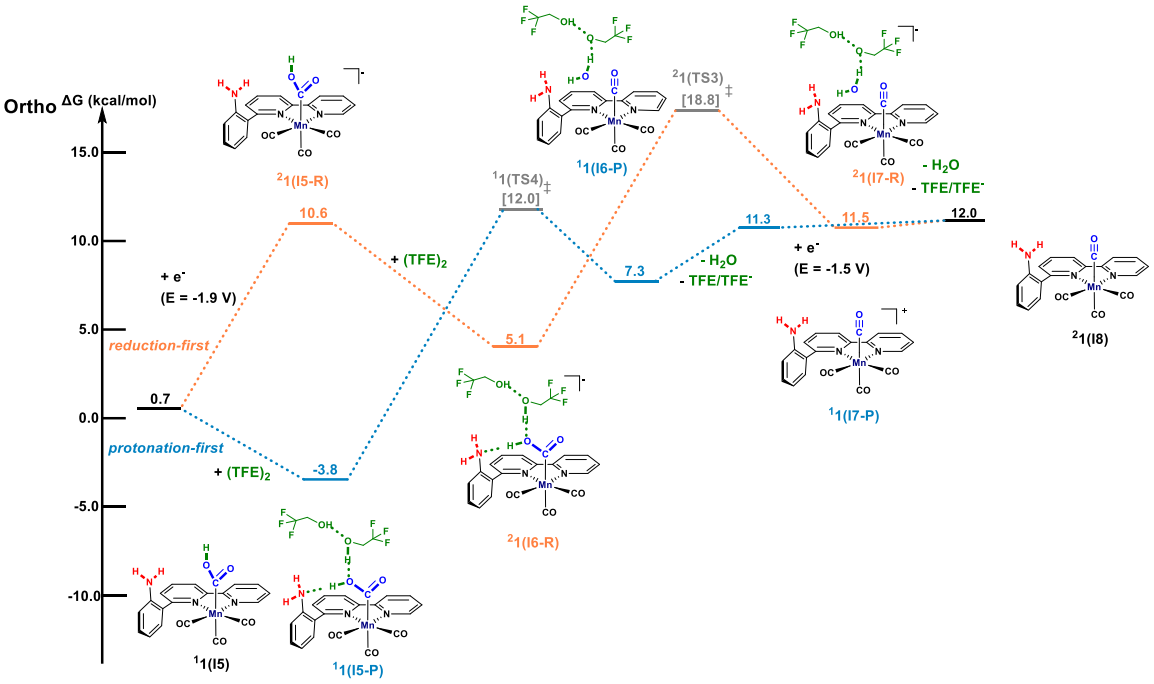

Figure 10. The computed Gibbs free energy values (in kcal/mol) and redox potential values (in V), reported against Fc^0/Fc^+, for the "protonation-first" and "reduction-first" pathways and final reduction at an overpotential of -1.47 V. This is considered the low overpotential regime. The plain Gibbs energy values were calculated using the ωB97X-D(SMD) level of theory.

During any of the protonation steps for the two different pathways, the energy for the protonation was downhill due to the stability effects created by the proton source. The hydrogen atoms on the protonation source, TFE, and the complex helped stabilize the reaction through hydrogen bonding interactions. The experimental work suggested using cyclic voltammetry that the "protonation-first" pathway would be the lower energy pathway for this reaction by looking at the catalytic current characteristic for the two possible pathways. However, this computation work shows that the "reduction-first" pathway may be lower in energy for most of the reaction by using the higher applied

potential. This becomes clear during the formation of the water molecule as the metallocarboxylic acid is protonated during the second protonation step of the "reduction-first" pathway. The formation of the water molecule has a lower activation energy barrier in this pathway than the "reduction-first" pathway, only 13.7 kcal/mol versus 15.8 kcal/mol in the high overpotential regime (**Figure 9**). The "reduction-first" pathway could be lower in energy due to the increased electron density on the metal center, facilitating the subsequent C-O bond cleavage and water release.

3.5 CO Release and Return to Active Species

Lastly, as mentioned in the previous sections, another reduction is performed on the tetracarbonyl intermediate **1(I8)** to release CO and return to the doubly reduced active catalyst species, **1(red-2)**. This redox potential was calculated to be -2.0 V versus Fc^0/Fc^+. At this point in the reaction, the catalytic cycle is completed and ready to begin again at the reintroduction of CO_2.

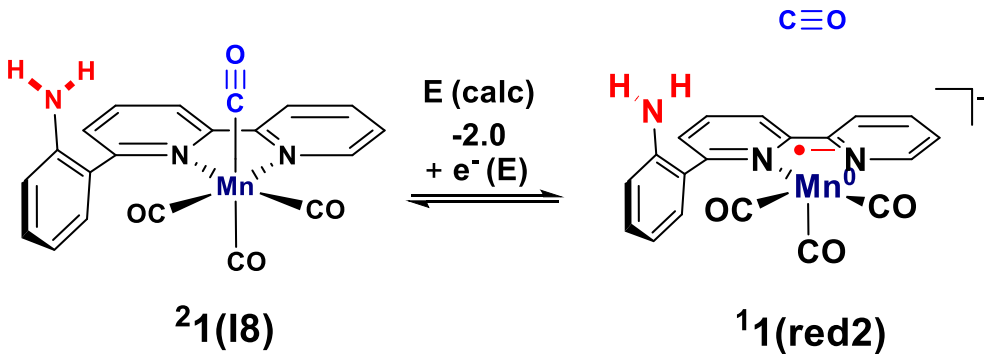

Figure 11. The computed redox potential values (in V) reported against Fc^0/Fc^+, for the final reduction to release CO and return to the active catalyst species.

Overall, this catalyst improves upon the previous parent compound, $Mn(bpy)(CO)_3Br$. This was due to the addition of the NH_2 group added to the secondary coordination sphere, as the hydrogen bonding effects stabilize the catalytic complex and create a lower barrier for CO_2 reduction to CO. For **1-Mn**, the position of the amine group improved the efficiency of the catalyst immensely due to the coordination of the hydrogen.

Our computational study also indicates the formation of the metallocarboxylate species (**1(TS1)**, $\Delta G^{\ddagger}$ = 11.7 kcal/mol, **Figure 8**) and C-O bond cleavage step for the "protonation-first" pathway (**1(TS4)**, $\Delta G^{\ddagger}$ = 12.0 kcal/mol, **Figure 9**) are competitive. However, the C-O bond cleavage step for the "reduction-first" path becomes more accessible at the high overpotential (**1(TS3)**, $\Delta G^{\ddagger}$ = 7.2 kcal/mol, **Figure 9**). In addition, the experimental TOF values are 901.4 s^{-1} at the high overpotential regime and 33.5 s^{-1} at the low overpotential regime.[2] The high overpotential regime had a TOF value similar to other manganese-based catalysts, showing that the "reduction-first" pathway is essential for CO_2RR for the catalysts in this series. This is consistent with our computational study where **1(TS3)** ("reduction-first" mechanism, $\Delta\Delta G^{\ddagger}$ = 13.7 kcal/mol related to the separated reactants) is kinetically more accessible than **1(TS4)** ("protonation-first" path, $\Delta\Delta G^{\ddagger}$ = 15.8 kcal/mol) under an applied potential of -1.95 V (**Figure 9**). Finally, we hypothesize that due to its highest computed Gibbs free energy, the transition state for forming the metallocarboxylate **1(TS1)** is the turnover determining transition state at the high overpotential (**1(TS1)**, $\Delta G^{\ddagger}$ = 11.7 kcal/mol *cf.* **1(TS3)**, $\Delta G^{\ddagger}$ = 7.2 kcal/mol).

3.6 HER Pathway Energy

One of the other possible products from this reaction is H_2, which comes from the competing hydrogen evolution reaction (HER). This reaction can happen when instead of CO_2 binding to the metal center, a proton from TFE binds to the metal center instead to give a metal-hydride intermediate. Experimentally, little H_2 formation would occur, no matter what concentration of **1-Mn** was used. The computational methods of this study can explain mechanistically why little H_2 formation occurs by using this catalyst.

Based on these calculations, it was found that the hydride species creates more hydrogen bonding interactions that stabilize the other atoms in the catalytic complex. This is seen by the decrease in energy as hydrogen binds to the metal center, -8.2 kcal/mol for the **1(I10)** species (**Figure 12**). However, the energy of the transition state, **1(TS5)**, has a computed Gibbs free energy of 12.6 kcal/mol. Thus, HER is less energetically favorable than CO_2 binding, with an energy of 11.7 kcal/mol (**1(TS1)**, **Figure 8**), suggesting that CO2RR is kinetically more accessible than HER. This is consistent with the experimental observation. Continuing the reaction, removing the conjugate base leaves the hydride species, **1(I11)**, with an energy of -4.6 kcal/mol. The calculated Gibbs free energies for forming the Mn-H species are shown in **Figure 12.**

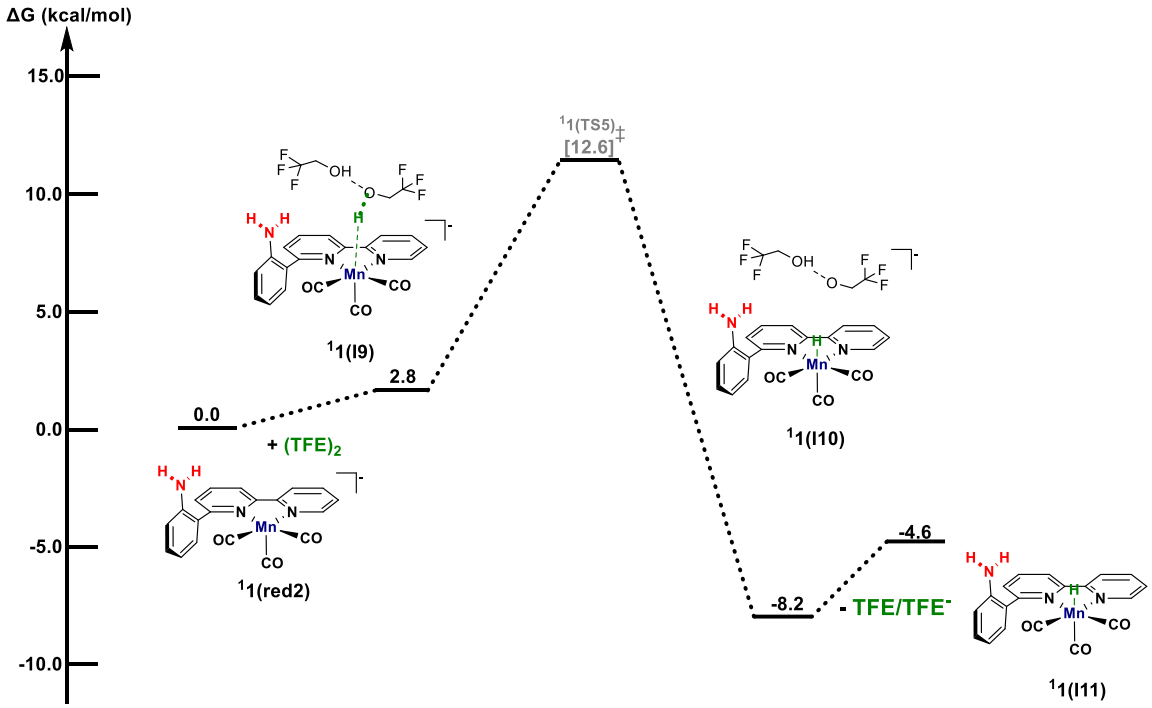

Figure 12. The computed Gibbs free energy values (in kcal/mol) for the HER. This is the first step of HER in which hydrogen binds to the metal center to create the hydride species, **1(I11)**. The plain Gibbs energy values were calculated using the ωB97X-D(SMD) level of theory.

The next step in HER is to form H_2. Looking at the "reduction-first" pathway, the primary reduction occurs at a voltage of -1.9 V, which causes a decrease in energy of the reduced hydride species to -6.6 kcal/mol (**1(I11-R)**, Figure 13). The addition of the proton source decreases the reaction energy once again to -8.6 kcal/mol. Following, the transition state energy, **1(TS6)**, was calculated to be 2.1 kcal/mol, and the forward reaction energy was found to be 1.6 kcal/mol. At this point in the reaction, the conjugate base is removed to leave the H_2 species, **1(I14)**. The removal of the conjugate base is slightly uphill at 6.1 kcal/mol. Finally, the reaction goes through a removal of the H_2 molecule and a return to the active catalyst species. This entire process is downhill, as the removal of H_2 to the

1(red1) species is -4.2 kcal/mol, and the reduction to **1(red2)** is -1.6 V versus Fc^0/Fc^+. The calculated energies and reduction values are displayed in **Figure 13**.

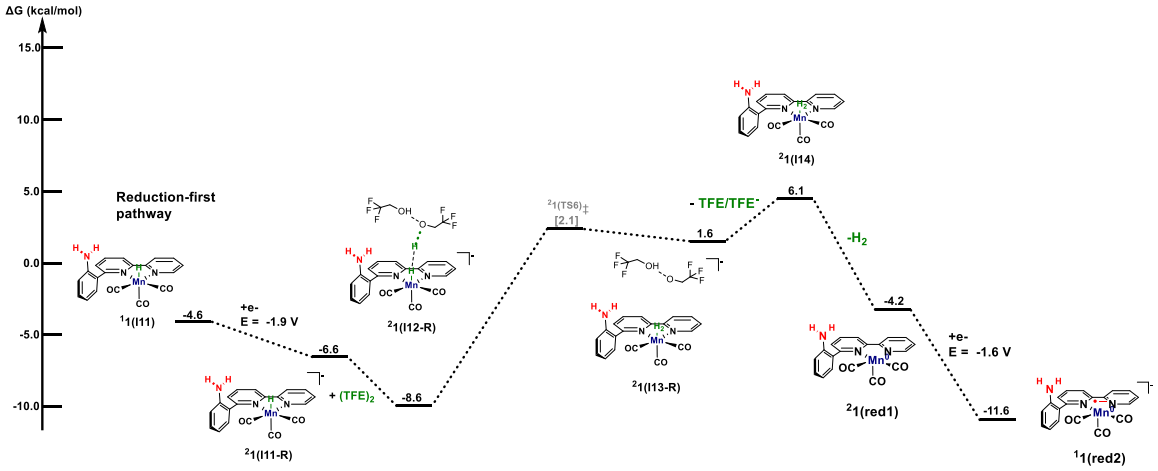

Figure 13. The computed Gibbs free energy values (in kcal/mol) and redox potential values (in V) reported against Fc^0/Fc^+, for the H_2 formation steps and the regeneration of the active catalyst. Gibbs free energies values were calculated using the ωB97X-D(SMD) level of theory.

Overall, our computational data shows that HER is kinetically less accessible (**1(TS5)**, ΔG = 12.6 kcal/mol, **Figure 12**) than CO_2RR using **1-Mn** (**1(TS1)**, ΔG = 11.7 kcal/mol, **Figure 8**) at the high overpotential regime. This confirms the selectivity of **1-Mn** for CO production, as shown in the experimental work.[2] Therefore, this catalyst is highly useful in suppressing the completing HER. The rest of the HER is lower in energy than CO_2RR, showing the importance of the catalyst reducing the energy barrier for CO_2 binding to suppress HER.

Finally, compared to the experimental work, these computational results are in good agreement with the experimental data. For example, the turnover numbers (TONs) for the products during catalysis were 121 for CO production and 6 for H_2 production using **1-Mn**.[2] This is consistent with the lower transition state energy for CO_2 binding (**1(TS1)**, $\Delta G^{\ddagger}$ = 11.7 kcal/mol) than the transition state energy for forming the Mn-H intermediate (**1(TS5)**, $\Delta G^{\ddagger}$ = 12.6 kcal/mol). Additionally, the highest turnover frequency values were seen at the high overpotential regime. This agrees with this computational data in that the "reduction-first" pathway is lower in energy ($\Delta\Delta G^{\ddagger}$ = 13.7 kcal/mol) than the "protonation-first" pathway ($\Delta\Delta G^{\ddagger}$ = 15.8 kcal/mol), as the "reduction-first" pathway was confirmed to occur at the high overpotential regime through the identifying curve in cyclic voltammetry. This lower energy pathway facilitates CO_2 reduction hence the turnover frequency (TOF) of 901.4s^{-1} for **1-Mn** determined experimentally, which is the highest of the three catalysts in this series. This compares favorably to other manganese-based homogenous catalysts. Overall, this computational work can help explain the results seen experimentally.[2]

4. Conclusion

In summary, this research project reported the mechanism for CO_2-to-CO conversion and the hydrogen evolution reaction (HER) for the $Mn(L)(CO)_3Br$ catalyst **1-Mn** using computational methods. This catalyst was able to reduce CO_2 most favorably through the "reduction-first" pathway to produce CO. However, the last step of the "reduction-first" pathway can have a large energy barrier depending on which overpotential is used for the reaction. The larger the overpotential, the lower the energy needed for the "reduction-first" pathway, making this last step more favorable. To conclude, **1-Mn** is an improvement upon the parent catalyst due to the addition and position of the $-NH_2$ group in the secondary coordination sphere.

Future research should focus on manganese-based catalysts, instead of the originally studied rhenium analogs, due to their increased catalytic activity, lower energy costs, and better impact on the environment in terms of the abundance of the material. Additionally, a larger basis set would be necessary for future research to decrease the possible errors from using smaller basis sets in our computational calculations. These errors could affect the amount of energy for each step in the mechanism, and so a larger basis set could be useful to reduce these errors. One basis set could be the Def2-TZVPP basis set, which uses two sets of polarized functions to increase the accuracy of the calculated data.

Additionally, further study of other functionalized ligands may yield catalysts with lower overpotentials and higher specificity for the desired product and should therefore be considered for future research. An abundant amount of previous research has been done on the ligand substitution method in other catalysts, such as iron porphyrin,[10] molybdenum,[11] rhenium,[12] and other manganese-based catalysts,[13] to increase the overall catalytic activity

while keeping the reduction potential minimal. For example, the -NH_2 ligand of **1-Mn** can be replaced by a -NH_3^+ group to study how this ligand may change the pathway of CO_2 reduction and how it may lower the amounts of energy needed during the reaction. Hopefully, this could create lower reduction potentials and higher catalytic activity. The -NH_3^+ ligand may achieve these goals in a few ways. Primarily, the electronic structure of the catalyst is changed by this ligand through the addition of an extra proton. Therefore, the electrostatic effects of this ligand may be used to yield a more optimal catalyst. These effects may increase catalytic structure by shifting the proton density to a different part of the catalyst and making specific binding or dissociation energies decrease. This ligand may also provide stabilization to the catalyst through increased hydrogen bonding interactions, which will reduce the overall amount of energy needed for CO_2RR. In addition to this, the extra proton may be an alternative source for the first protonation step of this reaction scheme. This would be beneficial, as the metallocarboxylic acid species can be formed without adding an external proton source to the reaction. With the use of this internal proton source, the protonation of CO_2 may be more favorable. However, these effects are not guaranteed to improve the catalytic activity. Determining if this catalyst is more efficient through computational and experimental methods could be an objective of a future research project.

Overall, this research shows the importance of using computational methods alongside experimental methods to confirm and expand upon results. In future research projects, these methods will allow many improvements to this group of catalysts, or other transition metal complexes, to increase their efficiency for CO_2RR over the competing

HER. This creation of more efficient catalysts will help to improve the environmental impacts of fossil fuels and create a circular fuel economy.

References:

(1) Appel, A. M.; Bercaw, J. E.; Bocarsly, A. B.; Dobbek, H.; DuBois, D. L.; Dupuis, M.; Ferry, J. G.; Fujita, E.; Hille, R.; Kenis, P. J. A.; Kerfeld, C. A.; Morris, R. H.; Peden, C. H. F.; Portis, A. R.; Ragsdale, S. W.; Rauchfuss, T. B.; Reek, J. N. H.; Seefeldt, L. C.; Thauer, R. K.; Waldrop, G. L., Frontiers, Opportunities, and Challenges in Biochemical and Chemical Catalysis of CO_2 Fixation. *Chem. Rev.* **2013,** *113*, 6621−6658.

(2) Roy, S. S.; Talukdar, K.; Jurss, J. W. Electro- and Photochemical Reduction of CO_2 by Molecular Manganese Catalysts: Exploring the Positional Effect of Second-Sphere Hydrogen-Bond Donors. *ChemSusChem* **2021**, *14*, 662−670.

(3) Dieterich, V.; Buttler, A.; Hanel, A.; Spliethoff, H.; Fendt, S. Power-to-Liquid via Synthesis of Methanol, DME or Fischer-Tropsch-Fuels: A Review. *Energy Environ. Sci.* **2020**, *13*, 3207−3252.

(4) Hawecker, J.; Lehn, J.-M.; Ziessel, R. Electrocatalytic Reduction of Carbon Dioxide Mediated by $Re(Bipy)(CO)_3Cl$ (Bipy = 2,2'-Bipyridine). *J. Chem. Soc., Chem. Commun.* **1984**, 328−330.

(5) Keith, J. A.; Grice, K. A.; Kubiak, C. P.; Carter, E. A. Elucidation of the Selectivity of Proton-Dependent Electrocatalytic CO_2 Reduction by Fac-$Re(Bpy)(CO)_3Cl$. *J. Am. Chem. Soc.* **2013**, *135*, 15823−15829.

(6) Bourrez, M.; Molton, F.; Chardon-Noblat, S.; Deronzier, A. [$Mn(Bipyridyl)(CO)_3Br$]: An Abundant Metal Carbonyl Complex a Efficient Electrocatalyst for CO_2 Reduction. *Angew. Chem. Int. Ed.* **2011**, *50*, 9903−9906.

(7) Kohn, W.; Becke, A. D.; Parr, R. G. Density Functional Theory of Electronic Structure. *J. Phys. Chem.* **1996**, *100*, 12974−12980.

(8) Davidson, E. R.; Feller, D. Basis Set Selection for Molecular Calculations. *Chem. Rev.* **1986**, *86*, 681–696

(9) Kozuch, S.; Shaik, S. How to Conceptualize Catalytic Cycles? The Energetic Span Model. *Acc. Chem. Res.* **2011**, *44*, 101–110.

(10) Davethu, P. A.; de Visser, S. P. CO_2 Reduction on an Iron-Porphyrin Center: A Computational Study. *J. Phys. Chem. A* **2019**, *123*, 6527–6535.

(11) Taylor, J. O.; Leavey, R. D.; Hartl, F.; Taylor, O.; Leavey, R. D.; Hartl, F. Solvent and Ligand Substitution Effects on the Electrocatalytic Reduction of CO_2 with [$Mo(CO)_4$ (x,x'-Dimethyl-2,2'-Bipyridine)] (x = 4-6) Enhanced at a Gold Cathodic Surface. *ChemElectroChem.* **2018**, *5*, 3155–3161.

(12) Li, X.; Panetier, J. A. Computational Study for CO_2-to-CO Conversion over Proton Reduction Using [$Re[bpyMe(Im-R)](CO)_3Cl]^+$ (R = Me, Me_2, and Me_4) Electrocatalysts and Comparison with Manganese Analogues. *ACS Catal.* **2021**, *11*, 12989−13000.

(13) Agarwal, J.; Shaw, T. W.; Stanton, C. J.; Majetich, G. F.; Bocarsly, A. B.; Schaefer, H. F. NHC-Containing Manganese(I) Electrocatalysts for the Two-Electron Reduction of CO_2. *Angew. Chem. Int. Ed.* **2014**, *53*, 5152–5155.